Contents lists available at ScienceDirect

Arabian Journal of Chemistry

journal homepage: www.ksu.edu.sa

Preparation of high-efficient $KMnO_4$ modified biochar for heavy metal removal from municipal wastewater

Fuhua Chang [a], Haoyu Li [b,*]

[a] School of Architectural Engineering, Zhengzhou Business University, Zhengzhou 451200, Henan, China
[b] College of Biological and Chemical Engineering (College of Agricultural Sciences), Panzhihua University, Panzhihua 617000, China

ARTICLE INFO

Keywords:
Adsorption mechanism
Cotton stem
High-efficient
$KMnO_4$
Pb(II)

ABSTRACT

$KMnO_4$-modified biochar (KM/biochar) derived from cotton stem is prepared with different cotton stem/$KMnO_4$ ratios for Pb(II) removal from wastewater. The characterization analysis indicates that KM/biochar has abundant surface functional groups and large surface area, contributing to Pb(II) removal. Pb(II) adsorption on KM/biochar can be accurately analyzed using the Pseudo-second order and Hill model. The maximum Pb(II) adsorption capacity of KM/biochar is 144.49 mg/g at pH of 5. Pb(II) adsorption on KM/biochar is spontaneous based on thermodynamics analysis with the enthalpy value of the 8.54 kJ/mol. Coexisted ions such as Na^+, K^+, Ca^{2+} and Mg^{2+} have slightly influenced on Pb(II) adsorption process. The regeneration experiment analysis indicates that KM/biochar shows excellent Pb(II) adsorption capacity after three cycles. The existence of CO2 can contribute to Pb(II) removal from wastewater. Pb(II) adsorption mechanism includes precipitation, cation exchange, electrostatic attraction and π-π interaction. These above analysis results indicate that the waste cotton stem can be converted into the high-efficient KM/biochar for Pb(II) removal from wastewater.

1. Introduction

The environmental pollution has become increasingly severe problem with rapid growth of the global population and economy (Qin et al., 2024; Yuan et al., 2023). The water pollution is one of the most serious problems among these pollutions (Mohd Faizal et al., 2024; Zhang et al., 2023). Pb(II) belongs to the toxic heavy metal ions, which comes from the electroplating and non-ferrous metal industry. Pb(II)-containing wastewater is endlessly discharged into the natural water body, which has already caused serious pollution to water body (Qi et al., 2024; Zhao et al., 2023). Besides, it also has been endangering the safety of drinking water (Meng et al., 2022). The maximum Pb(II) concentration in drinking water is the 10 μg/L in China (Guo et al., 2024). Therefore, Pb (II) should be strictly removed from wastewater for the safety of the ecosystem.

Pb(II) wastewater treatment methods includes the electrochemistry, chemical precipitation, membrane filtration, and adsorption (Das et al., 2024). Adsorption is considered as the promising potential technology for Pb(II) wastewater treatment due to low cost and simple operation (Wang et al., 2024a; Wang et al., 2024b). At present, many adsorption materials such as graphene oxide, activated carbon, carbon nanomaterials have been developed for Pb(II) wastewater treatment (Sağlam et al., 2023; Tan et al., 2023). Unfortunately, it is difficult to use in the actual industrial applications due to high production costs.

Biochar is a by-product of biomass pyrolysis process in the oxygen-free condition, which is considered as the potential adsorbent for wastewater treatment due to low price and easy to access (Guo et al., 2023; Su et al., 2024). The production cost of biochar is about $448.78 /t (Nematian et al., 2021). The production cost of the activated carbon and carbon nanotubes is about $42, 522/t and $4.41×10^8/t, respectively (El-Sheikh et al., 2008; Shawky et al., 2012). Compared with above adsorbents, the production cost of the biochar is low, which shows promising application potential in the Pb(II) wastewater treatment (Le et al., 2021). Wang et al. (2022) prepared the corn straw biochar at pyrolysis temperature of 700 °C, which is used to remove Pb(II) from wastewater with adsorption capacity of the 56.91 mg/g. Cheng et al. (2021) used the poplar saw dust as the feedstock to prepare the biochar for Pb(II) removal with adsorption capacity of 62.68 mg/g. However, the application of the original biochar without modification treatment for Pb(II) wastewater treatment is limited. It can be explained that the

Peer review under responsibility of King Saud University.
* Corresponding author.
E-mail address: lihypzhu@163.com (H. Li).

https://doi.org/10.1016/j.arabjc.2024.105756
Received 21 January 2024; Accepted 23 March 2024
Available online 26 March 2024

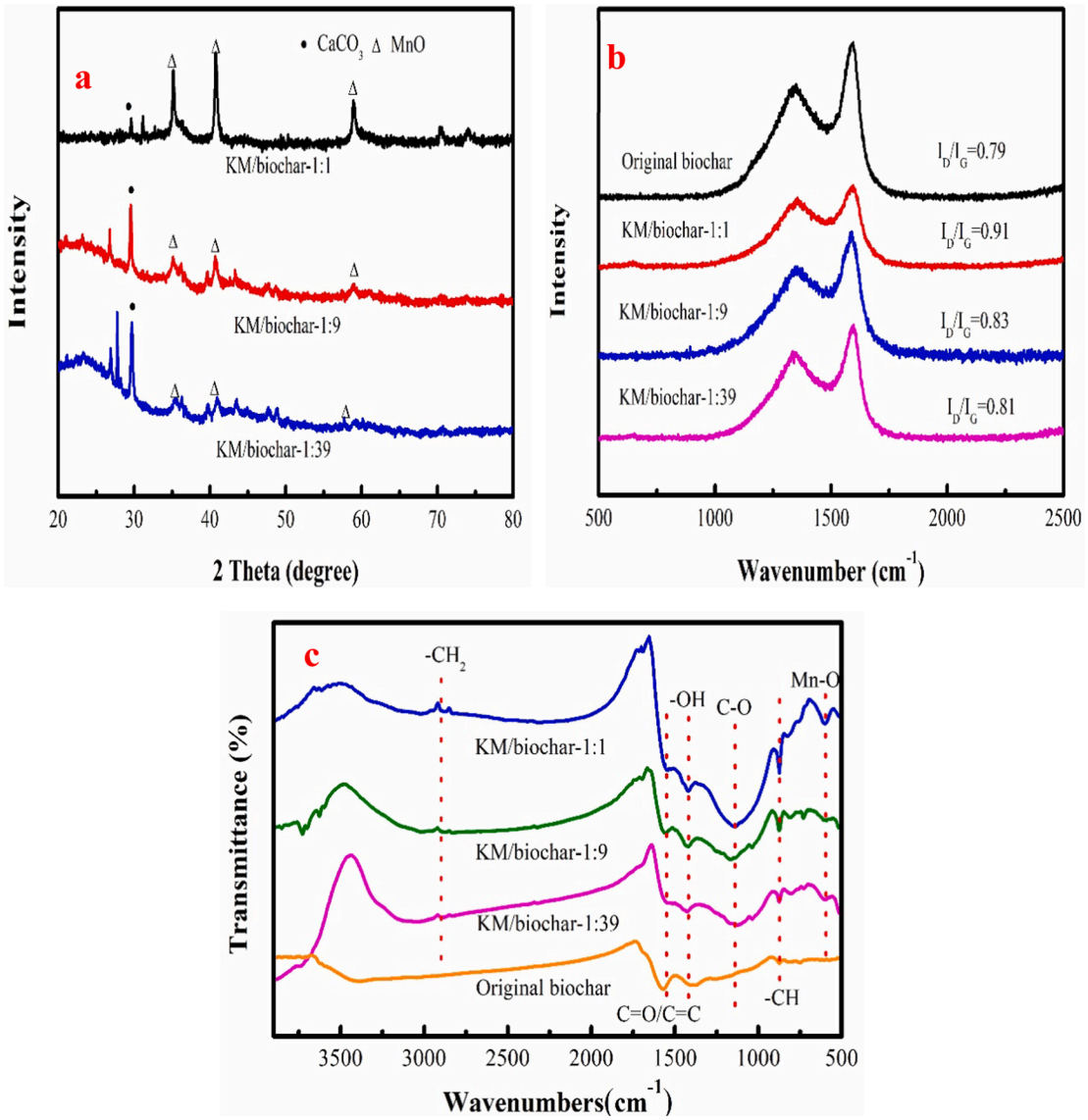

Fig. 1. XRD patterns of KM/biochar (a), Raman spectra of KM/biochar and original biochar (b), and FTIR spectra of the KM/biochar and original biochar (c).

original biochar has poor ion exchange capacity and underdeveloped pore structure, resulted in low Pb(II) adsorption capacity. Therefore, the adsorption performance of the original biochar should be improved by modification treatment.

Many scholars have developed several modification methods for improving Pb(II) adsorption capability of the original biochar. Ahmed et al. (2023) used the red mud to modify the rice straw to prepare the red mud modified biochar for achieving Pb(II) removal. Adsorption performance of the original biochar is improved with Pb(II) adsorbing capacity of the 426.84 mg/g. Cheng et al. (2022) used $MgCl_2{\cdot}6H_2O$ as the modification agent to prepare the MgO modified biochar, which is used in Pb(II) wastewater treatment with adsorption amount of the 384.08 mg/g. The Pb(II) adsorption capacity is significantly improved compared to the original biochar. The novel bacteria TJ6 immobilized on biochar is prepared by immobilization of wild resistant bacteria onto biochar for Pb(II) wastewater treatment with adsorption capacity of 250.10 mg/g (Wang et al., 2024c). Therefore, the adsorption performance of the original biochar is improved using the chemical modification method.

Liu et al. (2022) prepared the MnOx peanut shells derived biochar, which is used in Pb(II) wastewater treatment with adsorption capacity of 164.59 mg/g, which is 7.2 times than that of the original biochar. The MnOx particles are generated on the engineered biochar, which contributes to Pb(II) removal with adsorption capacity of 153.1 mg/g. Therefore, manganese oxides-based biochar could be used for Pb(II) removal from wastewater. Cotton stem is the agricultural waste, which is used to prepare the KM-biochar by pyrolysis in the existence of the $KMnO_4$ using one pot. Physicochemical properties of the KM-biochar are investigated and analyzed. Pb(II) adsorption behavior on KM-biochar is also investigated. The novelty of this work is that the waste cotton stem is converted into the high quality of KM-biochar in the existence of the $KMnO_4$ for Pb(II) removal, realizing high value utilization of waste cotton stem. Besides, the influence of CO2 on Pb(II) removal is investigated and analyzed. The main work includes the investigation of Pb(II) adsorption amount of the KM-biochar with different cotton stem/potassium permanganate ratio and analysis the Pb(II) adsorption mechanisms.

2. Materials and methods

2.1. Materials

Cotton stem (CS) was planted and collected from Henan Province, China. Lead nitrate and $KMnO_4$ were purchased from Tianjin Zhiyuan

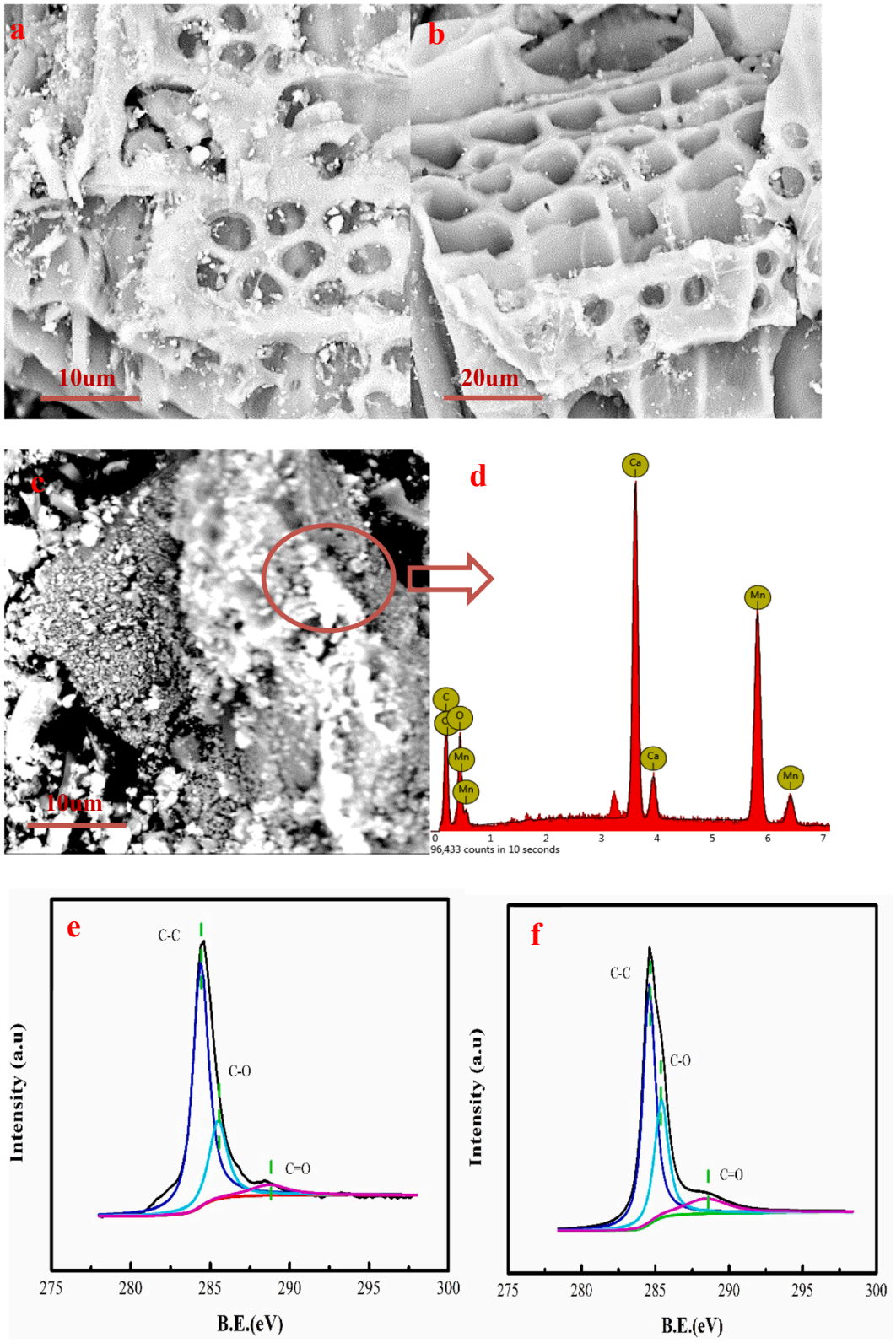

Fig. 2. The surface morphology and micro composition of KM/biochar-1:1(a-d), C 1 s XPS spectra of the original biochar (e) and KM/biochar-1:1 (f).

Chemical Reagent Co. Ltd.

2.2. Methods

The CS was added into $KMnO_4$ solution with the mass ratio of 1:1, 9:1 and 39:1, which was stirred and then dried. The 10 g dried precursor was heated at 600 °C in N_2 atmosphere for 1h using resistance furnace. Solid residue after heat treatment was named as the KM-biochar (KM-biochar-1:1/KM-biochar-9:1/ KM-biochar-39:1). 10 g CS without addition of $KMnO_4$ was heated at same condition to contrast with KM-biochar.

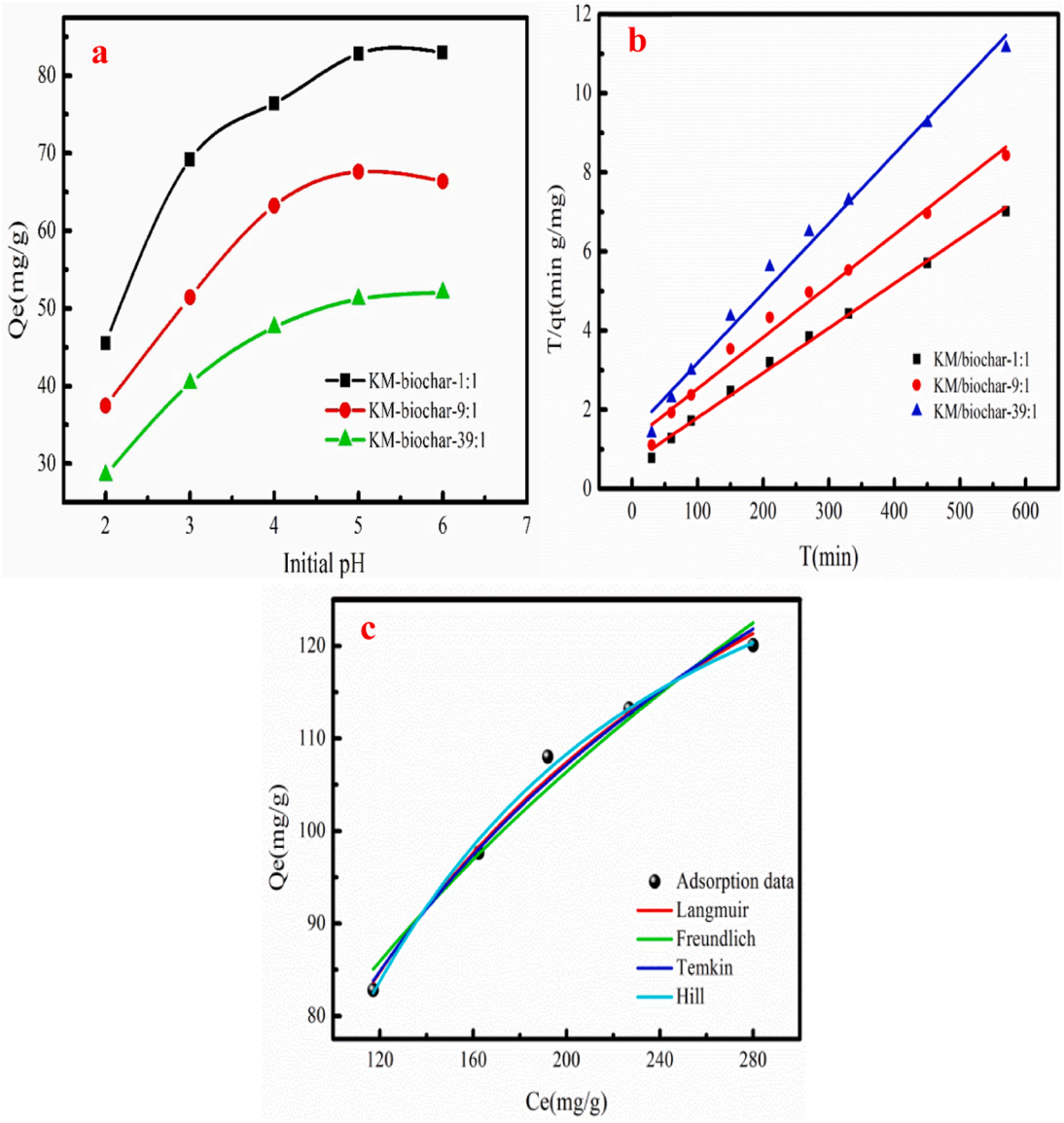

Fig. 3. Effect of pH on Pb(II) adsorption on KM/biochar (a), Pb (II) adsorption data fitting the Pseudo-second-order (b), and Pb(II) adsorption data fitting the adsorption isotherm models (c) (Dose of KM/biochar:0.05 g, Volume:50 mL, Pb^{2+} concentration: 200–350 mg/L, pH: 5).

2.3. Adsorption experiment

Effect of pH on Pb(II) removal was analyzed to get the desire pH value (2–6). In Pb(II) adsorption kinetic experiments, 0.2 g KM-biochar was added into the 200 mL Pb(II) solution with the concentration of the 200 mg/L. Pb(II) adsorption amounts of KM-biochar over time were investigated. In the adsorption isotherm experiments, 0.05 g KM-biochar was added into 50 mL different Pb(II) concentration solution (200–350 mg/L), which was stirred until adsorption equilibrium. Residual Pb(II) concentration was measured using atomic absorption spectrophotometer. Pb(II) adsorption capacity was calculated using the following Equation (1):

$$q = \frac{V(C_o - C_i)}{M} \quad (1)$$

Where C_o and C_i are the initial and residual concentrations (mg/L), respectively. M is the weight of KM/biochar (g). V is the adsorption solution volume (L). The involved adsorption kinetic and adsorption isotherm models were summarized in Table S1-S2 that were in supporting material.

3. Results and discussion

3.1. Characterizations of KM/biochar

Fig. 1a shows the X-ray diffraction (XRD) analysis of the KM/biochar. Where MnO appears on the surface of the KM/biochar with high characteristic peak intensity. Characteristic peak intensity of the MnO generally decreases as cotton stem/$KMnO_4$ ratio increases. This phenomenon indicates that $KMnO_4$ is decomposed into MnO on the KM/biochar. Besides, the characteristic peak of $CaCO_3$ is appeared on KM/biochar.

The peaks at 1350 and 1600 cm^{-1} correspond to the D band and G band that are disordered (Csp3) and graphitic (Csp2) carbon structures, respectively (Fig. 1b). I_D/I_G ratio of the original biochar is the 0.79, which is lower than that of the KM/biochar. This result proves that KM/biochar has large disordered degree after modification, indicating that $KMnO_4$ contributes to forming disordered structure. It also indicates that the new functional groups are formed on the KM/biochar. Fig. 1b also indicates that I_D/I_G ratio of the KM/biochar increases as $KMnO_4$ amount increases. The analysis reuslt indicates that large amount of the $KMnO_4$

Table 1
The calculated results of adsorption kinetics models.

Model	Parameter	Fitting results		
		KM/biochar-1:1	KM/biochar-9:1	KM/biochar-39:1
Pseudo-first order	qe.cal(mg/g)	74.19	62.34	46.14
	K_1(1/min)	0.016	0.009	0.012
	R^2	0.8175	0.8244	0.8063
Pseudo-second order	qe.cal(mg/L)	88.34	76.92	56.79
	K_2(g/mg min)	0.00019	0.00014	0.00022
	h(mg/mg. mi n)	0.9839	0.8102	0.7025
	R^2	0.9961	0.9839	0.9839
Intraparticle diffusion	C (mg/g)	43.64	33.87	19.91
	K_3 (mg/gmin$^{1/2}$)	0.9817	0.9614	0.9759
	R^2	144.49	105.26	88.15

Table 2
The calculated results of adsorption isotherm models.

Model	Parameter	Fitting results		
		KM/biochar-1:1	KM/biochar-9:1	KM/biochar-39:1
Langmuir	q_m(mg/g)	179.49	140.42	89.81
	K_L(L/mg)	0.0075	0.0073	0.0089
	R^2	0.9866	0.9715	0.9989
Freundlich	1/n	0.4188	0.3986	0.3335
	K_F((mg/g).(L/mg)$^{1/n}$)	11.57	9.99	9.76
	R^2	0.9626	0.9346	0.9879
Temkin	K_T (L/g)	0.0582	0.0582	0.0889
	B_T(J/mol)	43.64	33.87	19.91
	R^2	0.9817	0.9614	0.9759
Hill	Q_m	144.49	105.26	88.15
	n	1.5158	2.0477	1.039
	C	97.05	99.88	109.03
	R^2	0.9899	0.9939	0.9984

contributes to producing the disordered structure and functional groups.

Fig. 1c shows the FTIR spectra of KM/biochar and original biochar. The peak at about 2920 cm^{-1} is associated with the CH_2 deformation vibration, which is found on KM/biochar (Qin et al., 2023a). The broad band around 1560 cm^{-1} is the C=O/C=C group. The peak at around 1419 cm^{-1} is the v(–OH) vibration in hydroxyl groups (Shi et al., 2024). The intense bands at 1140 and 873 cm^{-1} are the C-O and C–H stretching of an aromatic compound (Huang et al., 2023). However, the new peak at 601 cm^{-1} is appeared on KM/biochar, which corresponds to the Mn-O group after modification with $KMnO_4$. The peak intensity of the oxygen-containing functional group of KM/biochar-1:1 is larger than that of the KM/biochar-1:9 and KM/biochar-1:39. This result indicates that high amount of $KMnO_4$ contributes to generation of the oxygen-containing functional group. Besides, peak intensities of the oxygen-containing functional group increase compared to the original biochar, indicating that oxygen-containing functional group content increases after modification. KM/biochar has lots of oxygen-containing functional group, which contributes to pollutions removal by complexation.

The surface area of KM/biochar is 257 m^2/g of the KM/biochar-1:39, 320 m^2/g of the KM/biochar-1:9 and 348 m^2/g of the KM/biochar-1:1, indicating that $KMnO_4$ contributes to producing pores. The KM/biochar-1:1 has the largest specific surface area, which is used as the representative KM/biochar for further analysis and application.

Fig. 2a-b presents surface microstructure of the KM/biochar-1:1. As Fig. 2a-b shown, many pores are formed in KM/biochar-1:1. Besides, the surface of the KM/biochar-1:1 has gray particulate matter. The gray particulate matter consists of C, O, Ca and Mn elements based on dispersive spectroscopy mapping analysis (Fig. 2c-d). The surface morphology and micro composition of the KM/biochar-1:9 and KM/biochar-1:39 are shown in the Fig.S1. The surface morphology is not good compared to KM/biochar-1:1. This result is consistent with the XRD analysis. The KM/biochar-1:1 and original biochar of the C 1 s XPS spectra have three peaks, which are C–C, C-O, and C = O groups (Fig. 2e-f). The C-O content of the KM/biochar-1:1 increases by 6.00 % compared to original biochar. The C = O content of the KM/biochar-1:1 increases by 5.55 % compared to the original biochar. The O element of the KM/biochar-1:1 increases by 4.87 %, based on XPS analysis, indicating that O content increases after $KMnO_4$ modification. XPS analysis results indicate that $KMnO_4$ contributes to the increase of C = O and C-O content. KM/biochar-1:1 is rich in oxygen-containing functional groups, contributing to Pb(II) removal from wastewater.

3.2. Influence of pH

Fig. 3a shows the Pb(II) adsorption amount of the KM-biochar at different pH. Pb(II) adsorption amount increases with increasing in pH value. High pH value contributes to Pb(II) adsorption. KM-biochar has low Pb(II) adsorption amount due to large H^+ concentration in the solution at low pH. It is not conductive to Pb(II) adsorption owe to strong competitive adsorption. H^+ concentration in the Pb(II) solution is decrease at high pH value, which contributes to Pb(II) adsorption owe to the weakness of the competitive adsorption. The precipitates will be formed at pH>5.5 (Cheng et al., 2023). Thus, the desire pH solution used in Pb(II) adsorption process is 5.

3.3. Adsorption kinetics

Pseudo-first order, Pseudo-second order and Intraparticle diffusion models are used to fit Pb(II) adsorption data. Table 1 lists the calculated results. As Table 1 shown, the correlation coefficient (R^2) values of Pb(II) adsorption data fitting Pseudo-second order are larger than other adsorption kinetics models. Besides, the $q_{e,cal}$ value calculated from Pseudo-second order are close to experimentally q_e value (equilibrium adsorption capacity). Therefore, Pseudo-second order can accurately describe the Pb(II) adsorption kinetic process. This result demonstrates that chemical adsorption influences Pb(II) adsorption process. The qe. cal value of the KM/biochar-1:1 is the largest than that of the KM-biochar-9:1 and KM-biochar-39:1. This result indicates that KM/biochar-1:1 has promising potential in Pb(II) removal from wastewater. The initial adsorption rate constant (h) values of KM/biochar-1:1, KM/biochar-9:1 and KM/biochar-39:1 are 0.9839, 0.8102 and 0.7025, respectively. As Table 1 shown, the h values of the KM/biochar are larger than that of the K_2 values, indicating that the Pb(II) adsorption rate of the KM/biochar gradually decreases as adsorption time increases. As Table 1 shown, the C values are not zero, demonstrating that Pb(II) adsorption on KM/biochar is not alone controlled by the Intraparticle diffusion. Fig. 3b shows the fitting adsorption kinetics curves.

3.4. Adsorption isotherms

Pb(II) adsorption behavior is investigated using the Langmuir, Freundlich, Temkin and Hill adsorption isotherm model. Table 2 lists the fitting results. The R^2 values of adsorption data fitting the Hill and Langmuir model are larger than other adsorption isotherm models (Table 2). The Pb(II) adsorption amounts of the KM/biochar-1:1, KM/biochar-9:1 and KM/biochar-39:1 are 144.49, 105.26 and 88.15 mg/g calculated from Hill model, respectively. Pb(II) adsorption amount of the fitting result is consistent with the experiment result. The n values calculated from Hill model of the KM/biochar-1:1, KM/biochar-9:1 and KM/biochar-39:1 are 1.5158, 2.0477 and 1.039, respectively, indicating that Pb(II) adsorption on KM/biochar has synergy. Pb(II) adsorption amount of the KM/biochar-1:1 is large compared to the KM/biochar-9:1 and KM/biochar-39:1. This result indicates that large amount of the $KMnO_4$ contributes to forming the oxygen-containing functional groups. Fig. 3c shows the fitting curves of the Pb(II) adsorption data fitting

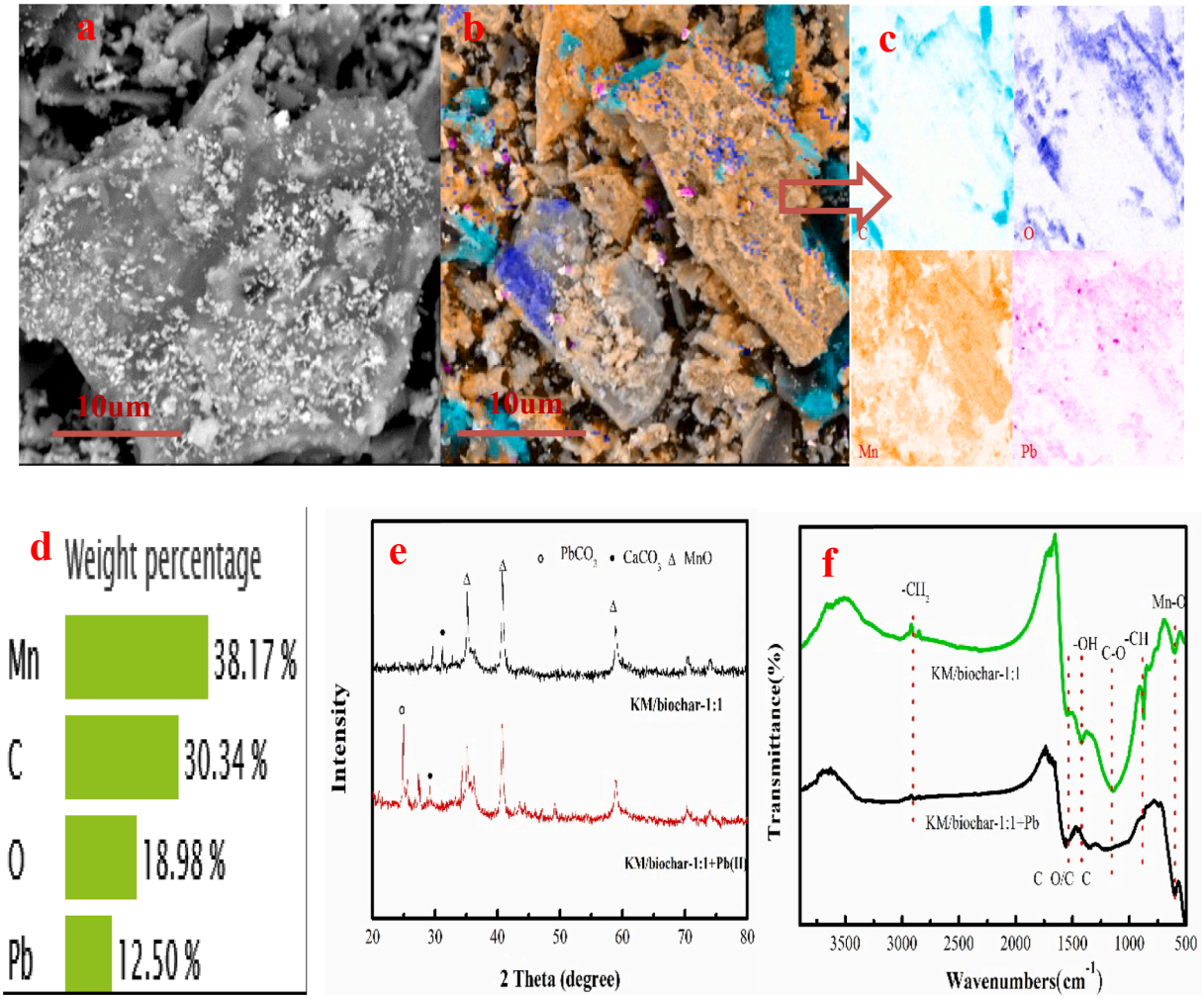

Fig. 4. SEM and EDS mapping images of KM/biochar-1:1 after Pb(II) adsorption (a-d), XRD pattern of KM/biochar-1:1 after Pb(II) adsorption (e), and FTIR of KM/biochar-1:1 before and after Pb(II) adsorption (f).

adsorption isotherm mode.

Feasibility adsorption Pb(II) on KM/biochar could be determined using the dimensionless factor R_L that can be obtained using following equation (Qin et al., 2023b):

$$RL = \frac{1}{1 + KLC0} \tag{2}$$

R_L values of Pb(II) adsorption on KM/biochar-1:1, KM/biochar-9:1 and KM/biochar-39:1 are 0.25–0.40, 0.26–0.41 and 0.22–0.36 respectively, indicating favorable Pb(II) adsorption on KM/biochar due to R_L <1.

The Pb(II) adsorption amount of the KM/biochar and original biochar is shown in Fig.S2. As Fig.S2 shown, the adsorption amount of the original biochar is low compared to the KM/biochar. This result confirms that $KMnO_4$ plays an important role in preparation process of the KM/biochar. This result indicates the feasibility of the KM/biochar preparation method. Table S3 lists Pb(II) adsorption amount of the similar adsorbents. As Table S3 shown, KM/biochar-1:1 has large Pb(II) adsorption amount compared to other adsorbents. Therefore, KM/biochar-1:1 is the promising adsorbent for Pb(II) removal from wastewater. KM/biochar-1:1 is used for further analysis and characterization due to large Pb(II) adsorption amount.

3.5. Adsorption thermodynamics studies

The entropy △S, enthalpy △H, and free energy △G are used to investigate the Pb(II) adsorption thermodynamic process, which are calculated using the following equation.

$$\ln Kd = \frac{\Delta S}{R} - \frac{\Delta H}{RT} \tag{3}$$

$$\Delta G = \text{ - } RT\ln(Kd) \tag{4}$$

$$K_d = \frac{q_e}{C_e} \tag{5}$$

The △G values of the Pb(II) (-0.92, −0.57, and −0.35 kJ/mol) are negative at 25–45 °C. Therefore, Pb(II) adsorption on KM/biochar-1:1 is feasible and spontaneous. Besides, Pb(II) adsorption on KM/biochar-1:1 is endothermic owe to △H value of the 8.54 kJ/mol. △S value of the Pb(II) adsorption on KM/biochar is 25.80 J/mol, which indicates increase of disorder and randomness at solid-solution interface. Fig.S3 shows Van't Hoff plot of ln K_d versus 1/T for the Pb(II) adsorption on KM/biochar-1:1.

3.6. Influence of coexisted ions

Fig.S4 shows the influence of coexisting ions on Pb(II) adsorption. As Fig.S4 shown, Na^+, K^+, $Ca^{2+}$and Mg^{2+} have a negligible effect on Pb(II)

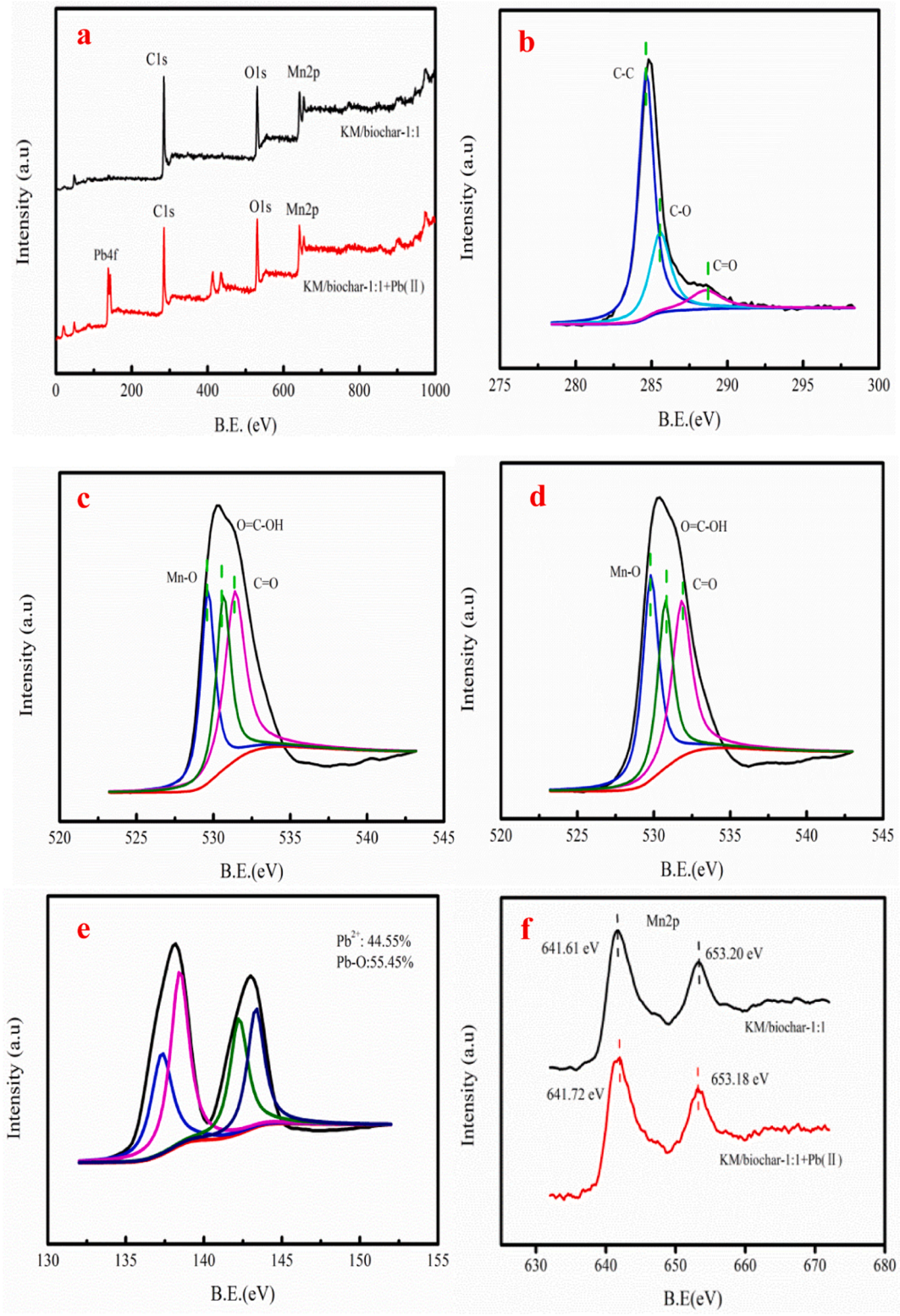

Fig. 5. The XPS spectra of the KM/biochar-1:1before and after Pb(II) adsorption (a), C1s XPS spectra after Pb(II) adsorption (b), O1s XPS spectra before and after Pb (II) adsorption (c-d), Pb4f spectra of after Pb(II) adsorption (e), and Mn2p spectra of KM/biochar-1:1 after Pb(II) adsorption (f).

removal. This can be explained that it is existence of the competitive adsorption on the KM/biochar-1:1 during Pb(II) adsorption process owe to the limitation of adsorption sites. However, KM/biochar-1:1 still has large Pb(II) adsorption amount.

3.7. Desorption and recyclability of KM/biochar-1:1

Fig.S5 shows the Pb(II) removal of KM/biochar-1:1 after regeneration. As Fig.S5 shown, Pb(II) removal is general decrease with increasing in cycle number. It can be explained that part of adsorption sites of KM/biochar-1:1 loses adsorption capacity after regeneration. KM/biochar-

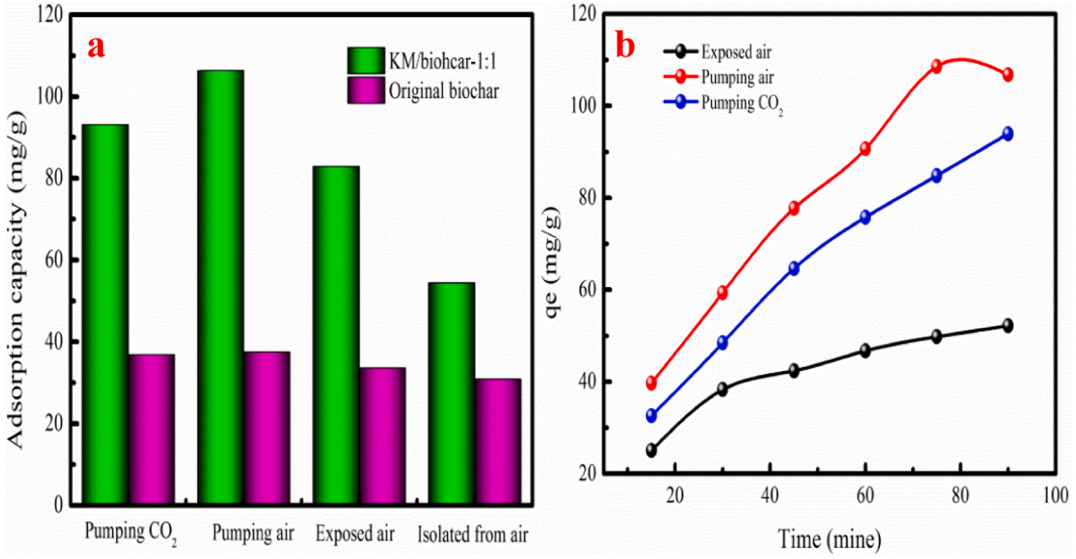

Fig. 6. Effect of CO_2 supply on Pb(II) adsorption capacity(a), Effect of CO_2 supply on Pb(II) adsorption rate (b)(Dose of KM/biochar-1:1:01 g, Volume:100 mL, Pb^{2+} concentration: 200 mg/L, pH: 5).

1:1 still has large Pb(II) adsorption amount after three cycles, which has promising potential in Pb(II) wastewater treatment.

3.8. Adsorption mechanism analysis

Fig. 4a-d shows the sem and eds mapping images of the KM/biochar-1:1 after Pb(II) adsorption. As Fig. 4a-b shown, the surface of KM/biochar-1:1 is covered with grayish-white granules. Pb(II) is captured on the KM/biochar-1:1 based on EDS analysis (Fig. 4b-d). As Fig. 4e shown, the grayish-white granule is further investigated using the XRD. Characteristic peaks of grayish-white granule have $PbCO_3$, which realizes Pb(II) removal from wastewater (Fig. 4e). Equations (6) explains the formation of the $PbCO_3$.

$$Pb^{2+} + CO_2 + H_2O \rightarrow PbCO_3 + H^+ \quad (6)$$

As Fig. 4f shown, the –CH group appears on KM/biochar-1:1 at 874 cm^{-1}, which can easily bind with Pb(II) to form Pb-π. However, the peak intensity of the –CH group become weaken after Pb(II) adsorption. This result indicates that Pb-π is formed on KM/biochar-1:1. CH_2 deformation vibration group is appeared at 2920 cm^{-1}. The peak intensity of the CH_2 group is decrease after Pb(II) adsorption, demonstrating the formation of Pb(II)-π on KM/biochar-1:1. Besides, peak intensity of Mn-O group also decreases after Pb(II) adsorption, demonstrating Mn-O group participation in Pb(II) adsorption. The peak intensity of C-O and –OH groups also decreases after Pb(II) adsorption, which indicates that oxygen-containing functional groups involve in Pb(II) adsorption.

Fig. 5a shows the XPS spectra of the KM/biochar-1:1 before and after Pb(II) adsorption, indicating the existence of Pb(II) on KM/biochar-1:1. This result demonstrates that Pb(II) is adsorbed on the KM/biochar-1:1. As Fig. 5b shown, the C 1s XPS spectrum of the KM/biochar-1:1 after Pb (II) adsorption has three peaks. C=O content of the KM/biochar-1:1 after Pb(II) adsorption decreases by 2.58%. Besides, the C-O content of the KM/biochar-1:1 decreases by 3.39 % after Pb(II) adsorption. These result demonstrate that oxygen-containing functional groups involve in Pb(II) adsorption. The O 1s XPS spectrum of the KM/biochar-1:1 also has three peaks after Pb(II) adsorption (Fig. 5c-d). The new peak is appeared at 529.2 eV, which is ascribed to the Mn-O group after $KMnO_4$ modification. However, the binding energy of Mn-O group is moved to large value because Mn-O group might involve in Pb(II) adsorption (Liu et al., 2022). The peak area of the Mn-O group decreases by 6.13% after Pb(II) adsorption. The reason might be that it produces new Pb-O group via Pb^{2+} replacing hydrogen atoms in O=C-OH on KM/biochar-1:1. Besides, peak area of C=O and O=C-OH group decreases by 5.46% and 1.67% after Pb(II) adsorption, respectively. Therefore, oxygen-containing functional groups involve in Pb(II) adsorption, which is in good agreement with the C 1s XPS spectrum analysis. The $Pb4f_{7/2}$ and $Pb4f_{5/2}$ peaks appear in the Pb4f spectrum of the KM/biochar-1:1. The corresponding proportions of the Pb^{2+} and Pb-O are 44.55% and 55.45%, respectively (Fig. 5e). The Mn2p XPS spectrum has two peaks, which correspond to the Mn^{2+} 2p3/2 (641.61) and Mn^{2+} 2p1/2 (653.20), respectively (Fig. 5f). However, the peak of the Mn^{2+} 2p3/2 and Mn^{2+} 2p1/2 has slightly changed after Pb(II) adsorption, demonstrating that it forms the Mn-OPb from the Mn-OH group.

The Pb(II) removal process involves in precipitation with minerals, complexation and π-π interactions based on XRD, FTIR and XPS analysis result. Besides, KM/biochar has large specific surface area, which can provide with lots of adsorption sites for Pb(II) adsorption by pore filling. KM/biochar also has the inorganic salt cations such as Ca^{2+}, K^+ and Na^+, which can realize Pb(II) removal from wastewater by the cation exchange reaction (Cheng et al., 2022).

3.9. Influence of CO_2

Several experiments are performed to demonstrate the formation of carbonates on KM/biochar-1:1. Four groups of Pb(II) solutions are employed to remove CO_2 from solution, and N_2 is pumped to completely remove CO_2. One group is sealed to isolate the CO_2, while another group is exposed to air, and the third group is pumped with 2% CO_2 using N_2 to analyze the influence of CO_2 on Pb(II) adsorption. In last group, air is pumped. KM/biochar-1:1 and the original biochar are added to the aforementioned solutions. Fig. 6a shows the results of the comparison experiments. KM/biochar-1:1 exhibits large Pb(II) adsorption capability when air is blown into the solution. In addition, KM/biochar-1:1 also has larger Pb(II) adsorption capability under the conditions of pumped CO_2 and exposed air than that of the isolated air. These results demonstrate that CO_2 contributes to Pb(II) removal. CO_2 from the air participates in the precipitation process as the main carbonate source during Pb(II) adsorption process, which is consistent with the adsorption mechanism analysis. However, if the solution is pumped with excess CO_2, Pb(II) removal is hindered, as excess CO_2 may increase the H^+ concentration of the solution. It hinders the precipitation of hydrocerussite. As Fig. 6b shown, the Pb(II) adsorption capacity of the KM/biochar-1:1 increases with increasing in adsorption time. Pb(II) adsorption on KM/biochar-1:1 quickly achieves adsorption equilibrium under CO_2 pumping conditions.

This phenomenon indicates that pumping CO_2 can accelerate Pb(II) adsorption on KM/biochar-1:1. This result indicates that pumping CO_2 can shorten the adsorption time and increase Pb(II)adsorption amount in the wastewater process.

4. Conclusion

KM/biochar derived from the cotton stem is successfully prepared in the existence of the $KMnO_4$ for Pb(II) removal from wastewater. Pseudo-second order and Hill equation can accurately describe Pb(II) adsorption process with Pb(II) adsorption capacities of 88.15–144.49 mg/g. Pb(II) adsorption on KM/biochar is spontaneous, based on adsorption thermodynamics analysis. Pb(II) adsorption on KM/biochar is slightly influenced by coexisted ions. The precipitation, cation exchange, electrostatic attraction and π-π interaction are responsible for Pb(II) adsorption, based on adsorption mechanism analysis.

CRediT authorship contribution statement

Fuhua Chang: Investigation, Methodology, Resources. **Haoyu Li:** Funding acquisition, Investigation, Visualization, Writing – original draft.

Declaration of competing interest

The authors declare that they have no known competing financial interests or personal relationships that could have appeared to influence the work reported in this paper.

Acknowledgements

The authors would like to express their gratitude to the Ph.D. Research Start-up Funding Project of Panzhihua University (bkqj2021009) and Innovation and entrepreneurship training program for college students (202311360015) for financial support.

Appendix A. Supplementary material

Supplementary data to this article can be found online at https://doi.org/10.1016/j.arabjc.2024.105756.

References

Ahmed, W., Mehmood, S., Mahmood, M., Ali, S., Shakoor, A., Núñez-Delgado, A., Asghar, R.M.A., Zhao, H., Liu, W., Li, W., 2023. Adsorption of Pb(II) from wastewater using a red mud modified rice-straw biochar: Influencing factors and reusability. Environ. Pollut. 326, 121405.

Cheng, S., Liu, Y., Xing, B., Qin, X., Zhang, C., Xia, H., 2021. Lead and cadmium clean removal from wastewater by sustainable biochar derived from poplar saw dust. J. Clean. Prod. 314, 128074.

Cheng, S., Zhao, S., Guo, H., Xing, B., Liu, Y., Zhang, C., Ma, M., 2022. High-efficiency removal of lead/cadmium from wastewater by MgO modified biochar derived from crofton weed. Bioresour. Technol. 343, 126081.

Cheng, S., Meng, W., Xing, B., Shi, C., Wang, Q., Xia, D., Nie, Y., Yi, G., Zhang, C., Xia, H., 2023. Efficient removal of heavy metals from aqueous solutions by Mg/Fe bimetallic oxide-modified biochar: Experiments and DFT investigations. J. Clean. Prod. 403, 136821.

Das, J., Rawat, A., Chaudhary, M., Maiti, A., Mohanty, P., 2024. Development of novel heteroatoms enriched nanoporous material for rapid removal of Pb(II) ions from water bodies by batch adsorption and cross-flow membrane filtration method. J. Water Process Eng. 58, 104823.

El-Sheikh, A.H., Sweileh, J.A., Al-Degs, Y.S., Insisi, A., Al-Rabady, N., 2008. Critical evaluation and comparison of enrichment efficiency of multi-walled carbon nanotubes, C18 silica and activated carbon towards some pesticides from environmental waters. Talanta 74 (5), 1675–1680.

Guo, H., Cheng, S., Xing, B., Meng, M., Feng, L., Nie, Y., Zhang, C., 2024. Preparation of three kinds of efficient sludge-derived adsorbents for metal ions and organic wastewater purification. Arab. J. Chem. 17 (4), 105671.

Guo, T., Zhang, Y., Geng, Y., Chen, J., Zhu, Z., Bedane, A.H., Du, Y., 2023. Surface oxidation modification of nitrogen doping biochar for enhancing CO_2 adsorption. Ind. Crop. Prod. 206, 117582.

Huang, Z., Fang, X., Wang, S., Zhou, N., Fan, S., 2023. Effects of $KMnO_4$ pre- and post-treatments on biochar properties and its adsorption of tetracycline. J. Mol. Liq. 373, 121257.

Le, P.T., Bui, H., Le, D.N., Nguyen, T.H., Pham, L.A., Nguyen, H.N., Nguyen, Q.S., Nguyen, T.P., Bich, N.T., Duong, T.T., Herrmann, M., Ouillon, S., Le, T.P.Q., 2021. Preparation and characterization of biochar derived from agricultural by-products for dye removal. Adsorpt. Sci. Technol. https://doi.org/10.1155/2021/9161904.

Liu, X., Li, D., Li, J., Wang, J., Liang, S., Deng, H., 2022. A novel MnOx-impregnated on peanut shells derived biochar for high adsorption performance of Pb(II) and Cd(II): Behavior and mechanism. Surf. Interfaces 34, 102323.

Meng, Z., Xu, T., Huang, S., Ge, H., Mu, W., Lin, Z., 2022. Effects of competitive adsorption with Ni(II) and Cu(II) on the adsorption of Cd(II) by modified biochar co-aged with acidic soil. Chemosphere 293, 133621.

Mohd Faizal, A.N., Putra, N.R., Abdul Aziz, A.H., Agi, A., Ahmad Zaini, M.A., 2024. Giant mud crab shell biochar: A promising adsorbent for methyl violet removal in wastewater treatment. J. Clean. Prod. 447, 141637.

Nematian, M., Keske, C., Ng'ombe, J.N. 2021. A techno-economic analysis of biochar production and the bioeconomy for orchard biomass. Waste management (New York, N.Y.), 135, 467-477.

Qi, X., Chen, Y., Liu, M., Zhang, X., Zuo, Y., Ma, Q., Xie, X., Guo, X., Wu, Y., 2024. Green and cost-effective: Bifunctional wood for efficient adsorption and sensitive detection of Pb(II). Ind. Crop. Prod. 210, 118162.

Qin, X., Cheng, S., Xing, B., Qu, X., Shi, C., Meng, W., Zhang, C., Xia, H., 2023a. Preparation of pyrolysis products by catalytic pyrolysis of poplar: Application of biochar in antibiotic wastewater treatment. Chemosphere 338, 139519.

Qin, X., Zeng, X., Cheng, S., Xing, B., Shi, C., Yi, G., Nie, Y., Wang, Q., Zhang, C., Xia, H., 2023b. Preparation of double functional carbon-based ZnO derived from rape straw for dye wastewater treatment. J. Water Process Eng. 52, 103588.

Qin, X., Tao, R., Cheng, S., Xing, B., Meng, W., Nie, Y., Zhang, C., Yu, J., 2024. Microwave-assisted one-pot method preparation of ZnO decorated biochar for levofloxacin and Cr(VI) removal from wastewater. Ind. Crop. Prod. 208, 117863.

Sağlam, S., Türk, F.N., Arslanoğlu, H., 2023. Use and applications of metal-organic frameworks (MOF) in dye adsorption: Review. J. Environ. Chem. Eng. 11 (5), 110568.

Shawky, H.A., El-Aassar, A., Abo-Zeid, D.E., 2012. Chitosan/carbon nanotube composite beads: Preparation, characterization, and cost evaluation for mercury removal from wastewater of some industrial cities in Egypt. J. Appl. Polym. Sci. 125 (S1), 93–101.

Shi, C., Wu, H., Wang, W., Zhao, J., Niu, F., Geng, J., 2024. Microplastic removal from water using modified maifanite with rotating magnetic field affected. J. Clean. Prod. 434, 140111.

Su, X., Wang, X., Ge, Z., Bao, Z., Lin, L., Chen, Y., Dai, W., Sun, Y., Yuan, H., Yang, W., Meng, J., Wang, H., Pillai, S.C., 2024. KOH-activated biochar and chitosan composites for efficient adsorption of industrial dye pollutants. Chem. Eng. J. 486, 150387.

Tan, M., Li, Y., Chi, D., Wu, Q., 2023. Efficient removal of ammonium in aqueous solution by ultrasonic magnesium-modified biochar. Chem. Eng. J. 461, 142072.

Wang, D., Chen, H., Xin, C., Yuan, Y., Sun, Q., Cao, C., Chao, H., Wu, T., Zheng, S., 2024c. Insight into adsorption of Pb(II) with wild resistant bacteria TJ6 immobilized on biochar composite: Roles of bacterial cell and biochar. Sep. Purif. Technol. 331, 125660.

Wang, X., Meng, L., Hu, M., Gao, L., Lian, B., 2024a. The competitive and selective adsorption of heavy metals by struvite in the Pb(II)-Cd(II)-Zn(II) composite system and its environmental significance. Water Res. 250, 121087.

Wang, Y., van Zwieten, L., Wang, H., Wang, L., Li, R., Qu, J., Zhang, Y., 2022. Sorption of Pb(II) onto biochar is enhanced through co-sorption of dissolved organic matter. Sci. Total Environ. 825, 153686.

Wang, Y., Nakano, T., Chen, X., Xu, Y.L., He, Y.J., Wu, Y.X., Zhang, J.Q., Tian, W., Zhou, M.H., Wang, S.X., 2024b. Studies on adsorption properties of magnetic composite prepared by one-pot method for Cd(II), Pb(II), Hg(II), and As(III): Mechanism and practical application in food. J. Hazard. Mater. 466, 133437.

Yuan, Q., Zhang, H., Qin, C., Zhang, H., Wang, D., Zhang, Q., Zhang, D., Zhao, J., 2023. Impact of emerging pollutant florfenicol on enhanced biological phosphorus removal process: Focus on reactor performance and related mechanisms. Sci. Total Environ. 859, 160316.

Zhang, H., Zhao, J., Fu, Z., Wang, Y., Guan, D., Xie, J., Zhang, Q., Liu, Q., Wang, D., Sun, Y., 2023. Metagenomic approach reveals the mechanism of calcium oxide improving kitchen waste dry anaerobic digestion. Bioresour. Technol. 387, 129647.

Zhao, J., Zhang, H., Guan, D., Wang, Y., Fu, Z., Sun, Y., Wang, D., Zhang, H., 2023. New insights into mechanism of emerging pollutant polybrominated diphenyl ether inhibiting sludge dark fermentation. Bioresour. Technol. 368, 128358.